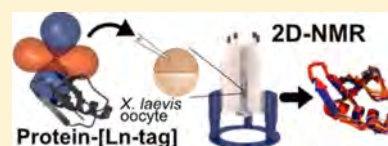


## In-Cell Protein Structures from 2D NMR Experiments

Thomas Müntener,<sup>†</sup> Daniel Häussinger,<sup>\*,†</sup> Philipp Selenko,<sup>‡</sup> and Francois-Xavier Theillet<sup>\*,‡,§</sup><sup>†</sup>Department of Chemistry, University of Basel, St. Johanns Ring 19, 4056 Basel, Switzerland<sup>‡</sup>Department of Structural Biology, Leibniz Institute of Molecular Pharmacology (FMP Berlin), Robert Roessle Straße 10, 13125 Berlin, Germany

## Supporting Information

**ABSTRACT:** In cell NMR spectroscopy provides atomic resolution insights into the structural properties of proteins in cells, but it is rarely used to solve entire protein structures *de novo*. Here, we introduce a paramagnetic lanthanide tag to simultaneously measure protein pseudocontact shifts (PCSs) and residual dipolar couplings (RDCs) to be used as input for structure calculation routines within the Rosetta program. We employ this approach to determine the structure of the protein G B1 domain (GB1) in intact *Xenopus laevis* oocytes from a single set of 2D in cell NMR experiments. Specifically, we derive well defined GB1 ensembles from low concentration in cell NMR samples ( $\sim 50 \mu\text{M}$ ) measured at moderate magnetic field strengths (600 MHz), thus offering an easily accessible alternative for determining intracellular protein structures.



Physical methods to delineate structural insights into the three dimensional properties of biomolecules such as X ray crystallography, NMR spectroscopy or electron microscopy, typically require experimental conditions and sample states that are vastly different from the crowded intracellular environments in which these molecules natively occur.<sup>1</sup> For these reasons, considerable effort is put into the development of biophysical methods to directly study biomolecules inside live cells. While high resolution X ray crystallography and single molecule electron microscopy are inherently excluded from such *in vivo* experiments, due to the requirement of crystalline or vitrified samples and the use of high energy X ray or electron beams to generate experimental data, solution NMR spectroscopy can provide nondestructive atomic resolution information on individual biomolecules in cells. Specifically, in cell NMR spectroscopy<sup>2,3</sup> takes advantage of the isotope labeling effect to selectively “visualize” isotope enriched, NMR active proteins, RNA or DNA against the backdrop of all other non isotope labeled and NMR inactive intracellular components. This enables direct NMR measurements under truly physiological *in vivo* conditions. Following this rationale, in cell NMR has been used to derive insights into intracellular protein conformations,<sup>4</sup> conformational equilibria,<sup>5</sup> folding and stability behaviors,<sup>6–8</sup> protein dynamics,<sup>9</sup> protein–protein, and quinary protein interactions,<sup>9,10</sup> physiological redox states,<sup>11</sup> metal binding properties<sup>12</sup> and post translational protein modifications.<sup>9,13,14</sup> By contrast, the use of in cell NMR to determine entire protein structures in live cells is generally hampered by the limited lifetimes of in cell NMR samples, their inherently low concentrations of intracellular, isotope enriched biomolecules (i.e., protein, RNA or DNA) and their concomitantly poor spectral qualities. Especially lengthy 3D and 4D NMR experiments—commonly used to derive long range distance restraints for calculating biomolecular structures—suffer from these drawbacks.<sup>15</sup> Several advances in NMR methods, including faster acquisition routines and nonuniform sampling

procedures<sup>16–18</sup> have helped to ameliorate some of these shortcomings and enabled the first and only intracellular protein structure to be determined by in cell NMR spectroscopy in bacteria, although at exceedingly high, nonphysiological intracellular protein concentrations in the millimolar range.<sup>4</sup> As a result, and given the general poor sensitivity of 3D and 4D NMR experiments even with such enhancing techniques, comprehensive structure determination efforts of proteins in live cells are deemed impractical and unfeasible. Here, we present an alternative approach to determine intracellular protein structures in live eukaryotic cells that solely relies on 2D NMR experiments and paramagnetic protein tagging to simultaneously induce pseudocontact shifts (PCSs) and residual dipolar couplings (RDCs). In turn, we demonstrate how these structural parameters suffice to calculate high precision in cell protein structures with the Rosetta program.

Tagging of proteins with different metals of the lanthanide series is known to induce strong metal specific distance and orientation dependent PCS effects on individual NMR active atomic nuclei.<sup>19,20</sup> Such PCSs serve as powerful long range distance restraints in structure calculation routines, and they can be derived from simple 2D NMR experiments, with different types of lanthanide binding protein tags (Figure 1a).<sup>21–24</sup> Optimizing the rigidity and linker lengths of individual tag structures also enables partial alignments of coupled proteins with respect to the external magnetic field, thus giving rise to measurable RDCs and, thereby, additional orientational restraints (Figure 1b).<sup>25–27</sup> In a first step, we designed a modified version of the classical tetraaza carboxylic DOTA chelator, known for its excellent metal coordinating properties, which we termed DOTA M7Py (Figure S1). This tag can be covalently coupled to the sulfhydryl moiety of

Received: May 18, 2016

Accepted: July 5, 2016

Published: July 5, 2016

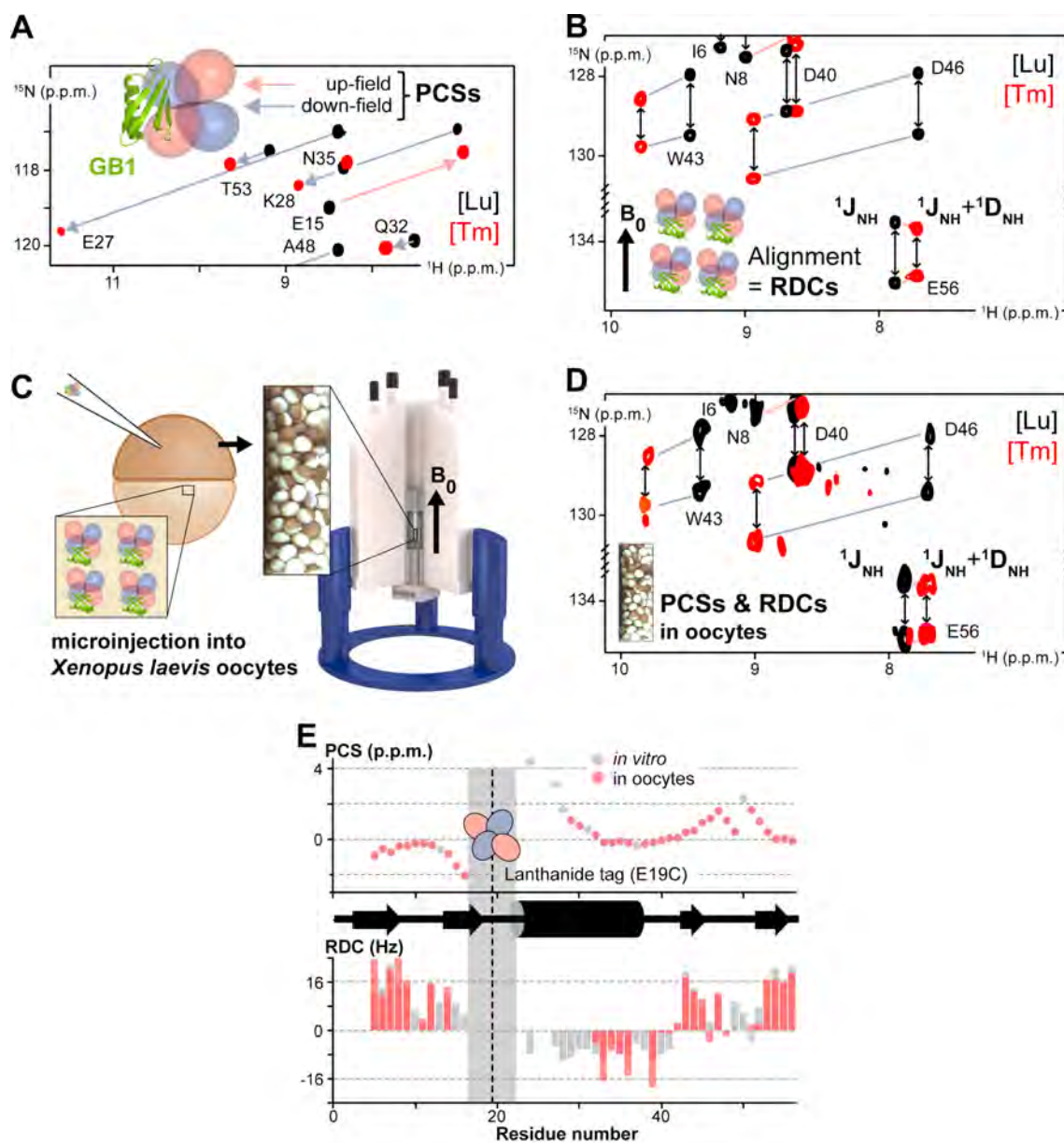


**Figure 1.** (A) Superposition of  $^1\text{H}$ - $^{15}\text{N}$  2D NMR spectra of purified GB1(E19C) coupled to DOTA M7Py carrying diamagnetic Lutetium (Lu, black) or paramagnetic Thulium (Tm, red). Pseudocontact shift (PCS) induced up- and downfield chemical shift changes are indicated (subset view). The inset depicts the GB1(E19C) ribbon structure (green) with paramagnetic iso surfaces drawn at 2 p.p.m. (blue and red) (B) Superposition of 2D IPAP HSQC spectra of GB1 with peak splitting due to amide scalar ( $^1J_{\text{NH}}$ ) and residual dipolar coupling (RDC, i.e.,  $^1D_{\text{NH}}$ ). Paramagnetic GB1 alignment with respect to the external magnetic field ( $B_0$ ) is shown schematically. (C) Overview of GB1 sample preparation in *Xenopus laevis* oocytes and (D) superposition of GB1 NMR spectra displaying in cell PCS and RDC effects (at 600 MHz). (E) Residue resolved quantification of *in vitro* and in cell PCS and RDC data at 293 K and 600 MHz.

cysteine residues forming a nonreducible thioether bond.<sup>28–30</sup> With regard to in cell PCS and RDC measurements, DOTA M7Py displays several attractive features. First, it is inherently rigid and adopts exclusively the square antiprismatic  $\Lambda(\delta\delta\delta\delta)$  stereoconfiguration for the 4S,3R Lu derivative.<sup>31</sup> Second, it is neutral after binding to lanthanide metals. Third, its linker portion is short, which reduces tag mobility and generates larger PCS effects, thus providing higher precision structural information. Fourth, it features both hydrophilic and hydrophobic properties (Figure S1), which augment stable positioning on most protein surfaces, further enhancing PCSs. Fifth, its thioether bond is expected to withstand the reducing

environment of the cytoplasm while maintaining DOTA's outstanding affinity toward lanthanide metals ( $K_d < 10^{-25}$  M).<sup>27</sup>

We initially prepared diamagnetic DOTA M7Py[Lu], and paramagnetic DOTA M7Py[Tm] and DOTA M7Py[Tb] complexes, which we coupled to the Streptococcal protein G B1 domain (GB1) via cysteine residues that we introduced by site directed mutagenesis at individual GB1 positions, i.e., E19C, K28C, and E42C. Using purified GB1 samples we recorded 2D  $^1\text{H}$ - $^{15}\text{N}$  HSQC spectra at 600 MHz, which revealed the expected PCS effects for the paramagnetic species (up to 6 p.p.m., Figure 1a; Figures S2 and S3; Table S1). We also detected strong cross peak splitting in 2D  $^1\text{H}$ - $^{15}\text{N}$  IPAP

HSQC spectra due to paramagnetic alignment of the GB1 domain and resulting RDC effects<sup>32</sup> (amplitudes reaching 25 Hz at 293 K, 600 MHz, Figure 1b; Figures S2 and S4; Table S2). In agreement with the temperature dependency of the tag's mobility, we obtained 30% higher or lower PCS and RDC values at 277 and 310 K, respectively (Tables S1 and S2). Moreover, NMR spectra of the different DOTA M7Py[Tm] tagged GB1 samples (E19C, K28C and E42C) revealed both positive and negative PCSs, as well as larger overall RDCs,<sup>19,20</sup> which is particularly useful for structure calculation routines. Therefore, we resorted to using DOTA M7Py[Tm] GB1 samples in all further experiments.

Next, we microinjected tagged GB1 carrying either diamagnetic (Lu) or paramagnetic metals (Tm) into *Xenopus laevis* oocytes for in cell NMR measurements.<sup>3,33,34</sup> We recorded 2D <sup>1</sup>H–<sup>15</sup>N HSQC spectra at effective NMR concentrations of ~25 μM (intracellular GB1 concentrations ~50 μM), which revealed PCSs that were virtually indistinguishable from the respective *in vitro* samples with an overall RMSD of 0.04 p.p.m., corresponding to 24 and 2.4 Hz in the <sup>1</sup>H and <sup>15</sup>N dimensions, respectively (Figure 1e; Figures S2, S5, and S6). We did not detect sample degradation or metal leakage for up to 24 h, thus indicating the excellent stability of metal loaded DOTA M7Py in *Xenopus* oocytes. Similarly, we measured in cell RDCs that were comparable to those obtained *in vitro* (Figure 1d,e, Figure S7, Tables S1 and S2). Because intracellular viscosity leads to faster T2 relaxation and, accordingly, enhanced <sup>15</sup>N signal decays, we chose to record in cell RDC experiments with the <sup>15</sup>N free induction decay (FID) resolution set to 36 Hz, as opposed to 17 Hz for RDC measurements *in vitro* (cf. Material and Methods). This resulted in average GB1 <sup>15</sup>N line widths of ~30 Hz, compared to ~12 Hz *in vitro*, which, concomitantly, increased the RMSD of RDCs measured *in vitro* versus in cells by 5 Hz, also explaining the larger differences of PCS and RDC RMSDs.

Finally, we used in cell PCS and RDC data as input for GPS Rosetta, a program that integrates PCSs from multiple paramagnetic centers into unified distance constraints in structure calculation routines.<sup>23</sup> Following the fragment based rationale used by Rosetta, we generated input libraries of 3 and 9 residue fragments of known protein structures, excluding the structure of GB1 and homologous folds. Using these fragments, we generated 10 000 GB1 structures, out of which we collected the 100 lowest energy models and compared their conformations to experimentally determined GB1 structures, i.e., X ray crystallography (PDB code: 2QMT<sup>35</sup>) and solution NMR (PDB code: 1GB1,<sup>36</sup> 2PLP<sup>37</sup>). We found poor convergence of individual models, with a median backbone Cα RMSD of 1.85 Å (Figure 2a). Next, we added a PCS based “weighting” function to steer GB1 models toward conformations that recapitulated the measured values. We used 72, 86, and 96 PCS constraints from the E19C, K28C, and E42C GB1 mutants, respectively, and obtained a substantially improved convergence of GB1 structures. The newly determined average Cα RMSD of the 100 lowest energy models was 0.98 Å and 0.64 Å between the closest model and the crystal structure (Figure 2b). Lastly, we used the RDC module of Rosetta to include measured RDCs as additional input in our structure calculation routines, which yielded a similar improved convergence of GB1 models (average Cα RMSD of 1.04 Å for the 100 lowest energy structures, 0.64 Å for the closest model and the X ray structure) (Figure 2c).

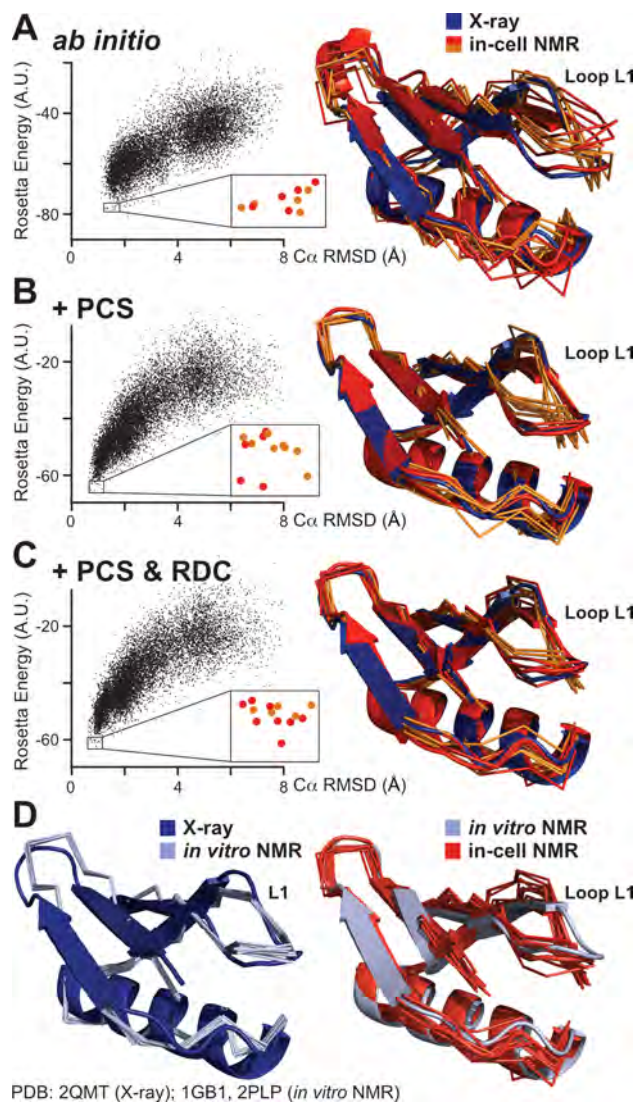


**Figure 2.** *In vitro* and in cell structures of GB1. Scatter plots depict Rosetta energy scores and Cα RMSDs of 10 000 GB1 models compared to the GB1 X ray structure (2QMT). Ten lowest energy structures are magnified and color coded according their loop L1 conformations (red/orange). A superposition of their structures with the crystal conformation (blue) is shown on the right. GB1 models with L1 conformations corresponding to the one of the GB1 crystal are shown in red, deviating L1 conformers are colored orange. (A) *Ab initio* GB1 models without using experimental restraints, (B) GB1 models calculated with PCS and (C) PCS+RDC input data. Rosetta energies contain different energy components and are not comparable. (D) Left: Superposition of high resolution *in vitro* solution NMR structures of isolated GB1, i.e., 2PLP<sup>37</sup> (dark blue, ribbon representation) and 1GB1<sup>36</sup> (light blue, ensemble representation). Right: Superposition of 2PLP (blue) and 10 lowest energy in cell GB1 models (PCS+RDC, red).

Upon closer inspection of the 10 lowest energy structures, we noticed a remarkable difference between structures obtained with PCS data alone and the ones for which PCS and RDC values were used. In both ensembles, loop L1 (residues N8 to E15) connecting strands β1 and β2 of GB1 displayed two distinct conformations. One identical to the X ray structure with an average Cα RMSD of 1.1 Å, and one with a larger Cα deviation and average RMSD of 1.6 Å. In PCS models, only three out of ten structures adopted the X ray L1 conformation.

In PCS+RDC models, five out of ten structures did. Previous solution NMR data indicated that L1 is highly flexible with backbone order parameters ( $S^2$ ) in the range of 0.5–0.6 ( $S^2$  of GB1 regions with secondary structure  $\sim 0.8$ ).<sup>37–40</sup> These *in vitro* solution conformations of L1 are similar to those observed in GB1 crystals with an L1 C $\alpha$  RMSD of 1.35 Å (Figure 2D). From this we concluded that combined PCS and RDC data from single 2D in cell NMR experiments are sufficient to determine well defined protein structures within PCS Rosetta. Our results further confirmed that the overall structural features of GB1 in *Xenopus* oocytes are similar to those observed *in vitro*.<sup>34</sup>

In summary, we show that in cell NMR derived PCS and RDC data suffice to solve a protein's structure inside cells. Whereas PCS effects decrease with the distance to the coordinated metal, RDCs are distance independent and offer valuable structural information for residues distal to the paramagnetic center. PCS and RDC data can jointly be obtained from single 2D NMR experiments on in cell NMR samples of low intracellular protein concentrations, measured at moderate magnetic field strengths, which makes them easily accessible and highly useful. The presented approach can further be used for determining glycan and nucleic acid structures,<sup>2,41</sup> as well as to probe ligand interactions.<sup>42</sup> In addition, the high rigidity of the DOTA M7Py tag renders it a useful tool for in cell EPR studies.<sup>43,44</sup> Given that the intracellular delivery of paramagnetically tagged proteins into cultured mammalian cells by electroporation is straightforward,<sup>9</sup> combined PCS and RDC measurements in live cells also hold great promise for future structure determination efforts in intact mammalian specimens.

## ■ ASSOCIATED CONTENT

### ● Supporting Information

The Supporting Information is available free of charge on the ACS Publications website at DOI: 10.1021/acs.jpclett.6b01074.

Material and Methods, and supporting figures and tables (PDF)

## ■ AUTHOR INFORMATION

### Corresponding Authors

\*E mail: daniel.haeussinger@unibas.ch.

\*E mail: francois.xavier.theillet@cnrs.fr.

### Present Address

<sup>§</sup>(F. X.T.) Department of Structural Biology, Institute of Integrative Biology of the Cell (I2BC) – UMR 9198, CNRS/CEA/Paris Saclay University, CEA Saclay Bât. 144, 91191 Gif sur Yvette, France.

### Notes

The authors declare no competing financial interest.

## ■ ACKNOWLEDGMENTS

This work was supported by the Agence Nationale pour la Recherche, Grant ANR 14 ACHN 0015 01 (FXT) and the Fondation Claude et Giuliana, Vaduz, Liechtenstein (T.M.). P.S. is supported by an ERC Consolidator Grant #647474 NeuroInCellNMR. We thank M. van Rossum for laboratory management, and H. Naumann for her kind hospitality. Calculations were performed at the sciCORE scientific computing core facility (<http://scicore.unibas.ch/>) at the University of Basel. Support by M. Jacquot and K. Arnold is gratefully acknowledged. We thank C. E. Housecroft and E. C.

Constable for helpful discussions and R. A. Byrd for providing chemicals.

## ■ REFERENCES

- (1) Theillet, F. X.; Binolfi, A.; Frembgen Kesner, T.; Hingorani, K.; Sarkar, M.; Kyne, C.; Li, C.; Crowley, P. B.; Gierasch, L.; Pielak, G. J.; et al. Physicochemical Properties of Cells and Their Effects on Intrinsically Disordered Proteins (IDPs). *Chem. Rev.* **2014**, *114*, 6661–6714.
- (2) Hänsel, R.; Luh, L. M.; Corbeski, I.; Trantirek, L.; Dötsch, V. In Cell NMR and EPR Spectroscopy of Biomacromolecules. *Angew. Chem., Int. Ed.* **2014**, *53*, 10300–10314.
- (3) Freedberg, D. I.; Selenko, P. Live Cell NMR. *Annu. Rev. Biophys.* **2014**, *43*, 171–192.
- (4) Sakakibara, D.; Sasaki, A.; Ikeya, T.; Hamatsu, J.; Hanashima, T.; Mishima, M.; Yoshimasu, M.; Hayashi, N.; Mikawa, T.; Wälchli, M.; et al. Protein Structure Determination in Living Cells by in Cell NMR Spectroscopy. *Nature* **2009**, *458*, 102–105.
- (5) Ye, Y.; Liu, X.; Xu, G.; Liu, M.; Li, C. Direct Observation of Ca<sup>2+</sup> Induced Calmodulin Conformational Transitions in Intact *Xenopus* Laevis Oocytes by 19 F NMR Spectroscopy. *Angew. Chem.* **2015**, *127*, 5418–5420.
- (6) Monteith, W. B.; Cohen, R. D.; Smith, A. E.; Guzman Cisneros, E.; Pielak, G. J. Quinary Structure Modulates Protein Stability in Cells. *Proc. Natl. Acad. Sci. U. S. A.* **2015**, *112*, 1739–1742.
- (7) Danielsson, J.; Mu, X.; Lang, L.; Wang, H.; Binolfi, A.; Theillet, F. X.; Bekei, B.; Logan, D. T.; Selenko, P.; Wennerstrom, H.; et al. Thermodynamics of Protein Destabilization in Live Cells. *Proc. Natl. Acad. Sci. U. S. A.* **2015**, *112*, 12402–12407.
- (8) Luchinat, E.; Barbieri, L.; Rubino, J. T.; Kozyreva, T.; Cantini, F.; Banci, L. In Cell NMR Reveals Potential Precursor of Toxic Species From SOD1 fALS Mutants. *Nat. Commun.* **2014**, *5*, 5502.
- (9) Theillet, F. X.; Binolfi, A.; Bekei, B.; Martorana, A.; Rose, H. M.; Stuiver, M.; Verzini, S.; Lorenz, D.; van Rossum, M.; Goldfarb, D.; et al. Structural Disorder of Monomeric A Synuclein Persists in Mammalian Cells. *Nature* **2016**, *530*, 45–50.
- (10) Majumder, S.; Xue, J.; DeMott, C. M.; Reverdatto, S.; Burz, D. S.; Shekhtman, A. Probing Protein Quinary Interactions by in Cell Nuclear Magnetic Resonance Spectroscopy. *Biochemistry* **2015**, *54*, 2727–2738.
- (11) Banci, L.; Barbieri, L.; Bertini, I.; Luchinat, E.; Secci, E.; Zhao, Y.; Aricescu, A. R. Atomic Resolution Monitoring of Protein Maturation in Live Human Cells by NMR. *Nat. Chem. Biol.* **2013**, *9*, 297–299.
- (12) Banci, L.; Barbieri, L.; Bertini, I.; Cantini, F.; Luchinat, E. In Cell NMR in *E. Coli* to Monitor Maturation Steps of hSOD1. *PLoS One* **2011**, *6*, e23561.
- (13) Selenko, P.; Frueh, D. P.; Elsaesser, S. J.; Haas, W.; Gygi, S. P.; Wagner, G. In Situ Observation of Protein Phosphorylation by High Resolution NMR Spectroscopy. *Nat. Struct. Mol. Biol.* **2008**, *15*, 321–329.
- (14) Binolfi, A.; Limatola, A.; Verzini, S.; Kosten, J.; Theillet, F. X.; May Rose, H.; Bekei, B.; Stuiver, M.; van Rossum, M.; Selenko, P. Intracellular Repair of Oxidation Damaged A Synuclein Fails to Target C Terminal Modification Sites. *Nat. Commun.* **2016**, *7*, 10251.
- (15) Rosato, A.; Vranken, W.; Fogh, R. H.; Ragan, T. J.; Tejero, R.; Pederson, K.; Lee, H. W.; Prestegard, J. H.; Yee, A.; Wu, Bin; et al. The Second Round of Critical Assessment of Automated Structure Determination of Proteins by NMR: CASD NMR 2013. *J. Biomol. NMR* **2015**, *62*, 413–424.
- (16) Waudby, C. A.; Christodoulou, J. An Analysis of NMR Sensitivity Enhancements Obtained Using Non Uniform Weighted Sampling, and the Application to Protein NMR. *J. Magn. Reson.* **2012**, *219*, 46–52.
- (17) Hyberts, S. G.; Robson, S. A.; Wagner, G. Exploring Signal to Noise Ratio and Sensitivity in Non Uniformly Sampled Multi Dimensional NMR Spectra. *J. Biomol. NMR* **2013**, *55*, 167–178.

- (18) Palmer, M. R.; Suiter, C. L.; Henry, G. E.; Rovnyak, J.; Hoch, J. C.; Polenova, T.; Rovnyak, D. Sensitivity of Nonuniform Sampling NMR. *J. Phys. Chem. B* **2015**, *119*, 6502–6515.
- (19) Otting, G. Protein NMR Using Paramagnetic Ions. *Annu. Rev. Biophys.* **2010**, *39*, 387–405.
- (20) Koehler, J.; Meiler, J. Expanding the Utility of NMR Restraints with Paramagnetic Compounds: Background and Practical Aspects. *Prog. Nucl. Magn. Reson. Spectrosc.* **2011**, *59*, 360–389.
- (21) Schmitz, C.; Vernon, R.; Otting, G.; Baker, D.; Huber, T. Protein Structure Determination From Pseudocontact Shifts Using ROSETTA. *J. Mol. Biol.* **2012**, *416*, 668–677.
- (22) Rinaldelli, M.; Ravera, E.; Calderone, V.; Parigi, G.; Murshudov, G. N.; Luchinat, C. Simultaneous Use of Solution NMR and X Ray Data in REFMAC5 for Joint Refinement/Detection of Structural Differences. *Acta Crystallogr., Sect. D: Biol. Crystallogr.* **2014**, *70*, 958–967.
- (23) Yagi, H.; Pilla, K. B.; Maleckis, A.; Graham, B.; Huber, T.; Otting, G. Three Dimensional Protein Fold Determination From Backbone Amide Pseudocontact Shifts Generated by Lanthanide Tags at Multiple Sites. *Structure* **2013**, *21*, 883–890.
- (24) Brewer, K. D.; Bacaj, T.; Cavalli, A.; Camilloni, C.; Swarbrick, J. D.; Liu, J.; Zhou, A.; Zhou, P.; Barlow, N.; Xu, J.; et al. Dynamic Binding Mode of a Synaptotagmin 1 SNARE Complex in Solution. *Nat. Struct. Mol. Biol.* **2015**, *22*, 555–564.
- (25) Salmon, L.; Blackledge, M. Investigating Protein Conformational Energy Landscapes and Atomic Resolution Dynamics From NMR Dipolar Couplings: a Review. *Rep. Prog. Phys.* **2015**, *78*, 126601.
- (26) Su, X. C.; McAndrew, K.; Huber, T.; Otting, G. Lanthanide Binding Peptides for NMR Measurements of Residual Dipolar Couplings and Paramagnetic Effects From Multiple Angles. *J. Am. Chem. Soc.* **2008**, *130*, 1681–1687.
- (27) Häussinger, D.; Huang, J. R.; Grzesiek, S. DOTA M8: an Extremely Rigid, High Affinity Lanthanide Chelating Tag for PCS NMR Spectroscopy. *J. Am. Chem. Soc.* **2009**, *131*, 14761–14767.
- (28) Liu, W. M.; Skinner, S. P.; Timmer, M.; Blok, A.; Hass, M. A. S.; Filippov, D. V.; Overhand, M.; Ubbink, M. A Two Armed Lanthanoid Chelating Paramagnetic NMR Probe Linked to Proteins via Thioether Linkages. *Chem. Eur. J.* **2014**, *20*, 6256–6258.
- (29) Toda, N.; Asano, S.; Barbas, C. F. Rapid, Stable, Chemoselective Labeling of Thiols with Julia Kociencki Like Reagents: a Serum Stable Alternative to Maleimide Based Protein Conjugation. *Angew. Chem., Int. Ed.* **2013**, *52*, 12592–12596.
- (30) Yang, Y.; Wang, J. T.; Pei, Y. Y.; Su, X. C. Site Specific Tagging Proteins via a Rigid, Stable and Short Thioether Tether for Paramagnetic Spectroscopic Analysis. *Chem. Commun.* **2015**, *51*, 2824–2827.
- (31) Opina, A. C. L.; Strickland, M.; Lee, Y. S.; Tjandra, N.; Andrew Byrd, R.; Swenson, R. E.; Vasalatiy, O. Analysis of the Isomer Ratios of Polymethylated DOTA Complexes and the Implications on Protein Structural Studies. *Dalton Trans.* **2016**, *45*, 4673–4687.
- (32) Ottiger, M.; Delaglio, F.; Bax, A. Measurement of J and Dipolar Couplings From Simplified Two Dimensional NMR Spectra. *J. Magn. Reson.* **1998**, *131*, 373–378.
- (33) Hänsel, R.; Luh, L. M.; Corbeski, I.; Trantirek, L.; Dötsch, V. In Cell NMR and EPR Spectroscopy of Biomacromolecules. *Angew. Chem., Int. Ed.* **2014**, *53*, 10300–10314.
- (34) Selenko, P.; Serber, Z.; Gadea, B.; Ruderman, J.; Wagner, G. Quantitative NMR Analysis of the Protein G B1 Domain in *Xenopus Laevis* Egg Extracts and Intact Oocytes. *Proc. Natl. Acad. Sci. U. S. A.* **2006**, *103*, 11904–11909.
- (35) Frericks Schmidt, H. L.; Sperling, L. J.; Gao, Y. G.; Wylie, B. J.; Boettcher, J. M.; Wilson, S. R.; Rienstra, C. M. Crystal Polymorphism of Protein GB1 Examined by Solid State NMR Spectroscopy and X Ray Diffraction. *J. Phys. Chem. B* **2007**, *111*, 14362–14369.
- (36) Gronenborn, A. M.; Filpula, D. R.; Essig, N. Z.; Achari, A.; Whitlow, M.; Wingfield, P. T.; Clore, G. M. A Novel, Highly Stable Fold of the Immunoglobulin Binding Domain of Streptococcal Protein G. *Science* **1991**, *253*, 657–661.
- (37) Bouvignies, G.; Meier, S.; Grzesiek, S.; Blackledge, M. Ultrahigh Resolution Backbone Structure of Perdeuterated Protein GB1 Using Residual Dipolar Couplings From Two Alignment Media. *Angew. Chem., Int. Ed.* **2006**, *45*, 8166–8169.
- (38) Shapiro, Y. E.; Meirovitch, E. Slowly Relaxing Local Structure (SRLS) Analysis of <sup>15</sup>N H Relaxation From the Prototypical Small Proteins GB1 and GB3. *J. Phys. Chem. B* **2012**, *116*, 4056–4068.
- (39) Lamley, J. M.; Lougher, M. J.; Sass, H. J.; Rogowski, M.; Grzesiek, S.; Lewandowski, J. R. Unraveling the Complexity of Protein Backbone Dynamics with Combined (<sup>13</sup>C and (<sup>15</sup>N Solid State NMR Relaxation Measurements. *Phys. Chem. Chem. Phys.* **2015**, *17*, 21997–22008.
- (40) Vögeli, B.; Kazemi, S.; Güntert, P.; Riek, R. Spatial Elucidation of Motion in Proteins by Ensemble Based Structure Calculation Using Exact NOEs. *Nat. Struct. Mol. Biol.* **2012**, *19*, 1053–1057.
- (41) Canales, Á.; Mallagaray, Á.; Berbis, M. Á.; Navarro Vázquez, A.; Domínguez, G.; Cañada, F. J.; André, S.; Gabius, H. J.; Pérez Castells, J.; Jiménez Barbero, J. Lanthanide Chelating Carbohydrate Conjugates Are Useful Tools to Characterize Carbohydrate Conformation in Solution and Sensitive Sensors to Detect Carbohydrate–Protein Interactions. *J. Am. Chem. Soc.* **2014**, *136*, 8011–8017.
- (42) Guan, J. Y.; Keizers, P. H. J.; Liu, W. M.; Lohr, F.; Skinner, S. P.; Heeneman, E. A.; Schwalbe, H.; Ubbink, M.; Siegal, G. Small Molecule Binding Sites on Proteins Established by Paramagnetic NMR Spectroscopy. *J. Am. Chem. Soc.* **2013**, *135*, 5859–5868.
- (43) Martorana, A.; Bellapadrona, G.; Feintuch, A.; Di Gregorio, E.; Aime, S.; Goldfarb, D. Probing Protein Conformation in Cells by EPR Distance Measurements Using Gd 3+Spin Labeling. *J. Am. Chem. Soc.* **2014**, *136*, 13458–13465.
- (44) Bleicken, S.; Jeschke, G.; Stegmüller, C.; Salvador Gallego, R.; García Sáez, A. J.; Bordignon, E. Structural Model of Active Bax at the Membrane. *Mol. Cell* **2014**, *56*, 496–505.